ROBUST DETECTION OF POLYMORPHIC NQR SIGNALS

Naveed R. Butt[†] *, Samuel D. Somasundaram*[‡] *and Andreas Jakobsson*[†]

[†] Karlstad University, Department of Electrical Engineering, SE-651 88 Karlstad, Sweden
[‡] King's College London, Division of Engineering, Strand, London WC2R 2LS, UK

ABSTRACT

Nuclear quadrupole resonance (NQR) is a non-invasive, solid state, radio frequency (RF) technique, able to distinguish between polymorphic forms of certain compounds. Exploiting the signals from multiple polymorphs is important in explosives detection, whilst quantifying these polymorphs is important in pharmaceutical applications. Recently proposed hybrid algorithms, able to process the signals from multiple polymorphs, assume the amplitudes associated with each polymorph are known to within a scaling. Any error in this a priori information will lead to performance degradation in these algorithms. In this paper, we develop a robust hybrid algorithm allowing for uncertainties in the assumed amplitudes, extending a recently proposed robust algorithm formulated for single polymorphs to process signals from multiple polymorphs. Extensive numerical investigations indicate that the proposed algorithm provides significant performance gains as compared to both the existing hybrid algorithms, when uncertainties in the amplitudes exist, and existing robust algorithms, when there are multiple polymorphs.

1. INTRODUCTION

Nuclear quadrupole resonance (NQR) is a non-invasive radio frequency (RF) spectroscopic technique, able to detect unique signals from solid state compounds containing quadrupolar nuclei[1], thus making it attractive to both detection and pharmaceutical applications [1, 2, 3]. Furthermore, the technique is able to distinguish between different polymorphic forms of certain compounds. Being able to exploit the signals from multiple polymorphs is important in explosives detection, whilst being able to quantify polymorphs is important in certain pharmaceutical applications.

Recently, we have proposed various approximate maximum likelihood (AML) based detectors that examine signals from a single polymorph, herein termed non-hybrid detectors [4, 5, 6]. The aforementioned detectors assume that the (complex) amplitudes of the spectral lines are known to within a (complex) scaling, i.e., they assume that the relative amplitudes are known *a priori*. In practical scenarios, there are many factors that contribute to differences between the assumed relative amplitudes, obtained under controlled conditions, and the ones observed [7, 8, 9]. Such differences lead to a degradation in performance of these algorithms. To alleviate this problem we recently proposed a *robust* algorithm able to exploit prior information on the amplitudes, while also allowing for uncertainty in them [8, 9]. This robust algorithm finds the amplitude vector within an uncertainty hypersphere around an assumed amplitude vector, allowing for a more precise fit to the observed data. Here, the radius of the uncertainty hypersphere is a user defined parameter, determined via simulations from the prior knowledge concerning the amplitudes. All of the aforementioned detectors are only able to exploit signals from a single polymorph. In [10, 11], a *hybrid* detector able to exploit signals from multiple polymorphs was proposed; however, this algorithm does not provide robustness to uncertainties in the assumed relative amplitudes. Here, we merge these problem formulations, presenting a robust hybrid detector able to exploit signals from multiple polymorphs, whilst also providing robustness to uncertainties in the prior knowledge of the amplitudes associated with each polymorph. Given both the assumed relative amplitudes and the statistics of the amplitude errors, the algorithm first estimates the relative proportions of the polymorphs by solving a stochastic robust approximation problem. Given these proportion estimates, it is then possible to obtain a robust estimate of the relative amplitudes associated with each polymorph, using a method reminiscent of the one presented in [8, 9]. Furthermore, following previous approaches [5, 6, 8, 9, 10, 11], we form the detector in the frequency domain, selecting only those frequencies where we expect the NQR signal to lie. As a result, both the computational complexity of the algorithm is reduced and its robustness to residual RF interference increased. The resulting detector is termed the Robust Estimation of MultIple polymorph QR Signals (REMIQS) detector.

A word on notation: $(\cdot)^T$, $(\cdot)^*$ and $E\{\cdot\}$ are used to represent the transpose, the conjugate transpose and the expectation, respectively. The Moore-Penrose pseudoinverse is represented by $(\cdot)^\dagger$. The kth index of a vector is denoted by $[\cdot]_k$ and its two-norm by $\|\cdot\|_2$. Finally, $\mathrm{diag}\{\mathbf{x}\}$ is used to represent a diagonal matrix, formed with the vector $\mathbf{x}$ along its diagonal.

2. DATA MODEL ALLOWING FOR UNCERTAINTY

As shown in [10, 11], the mth NQR echo, from a sample containing P polymorphs, can be expressed as

$$y_m(t) = \sum_{p=1}^{P} \gamma_p y_m^{(p)}(t) + w_m(t), \tag{1}$$

where γ_p denotes the proportion of the pth polymorph, $w_m(t)$ is an additive *coloured* noise (for a detailed discussion on the colour of the additive noise see [4]), and $y_m^{(p)}(t)$ represents the mth echo produced by the pth polymorph, which can be well modelled as [6]

$$y_m^{(p)}(t) = \sum_{k=1}^{d^{(p)}} \alpha_k^{(p)} e^{-(t+m\mu)\eta_k^{(p)}} e^{-\beta_k^{(p)}|t-t_{sp}|+i\omega_k^{(p)}(T)t}, \tag{2}$$

where $t = t_0, \ldots, t_{N-1}$ represents the echo sampling time; $m = 0, \ldots, M-1$ is the echo number; t_{sp} is the time between the centre of the refocusing pulse[2] and the echo centre; $\mu = 2t_{sp}$ denotes the echo spacing and T is the temperature of the examined sample. Additionally, for the kth spectral component of the pth polymorph, $\omega_k^{(p)}(T)$, $\alpha_k^{(p)}$, $\beta_k^{(p)}$ and $\eta_k^{(p)}$ denote the (temperature dependent) frequency shifting function, the (complex) amplitude, the sinusoidal damping constant and the echo train damping constant, respectively. An important point to note is that the number of sinusoidal components, $d^{(p)}$ may be assumed to be *known*, whereas the examined sample temperature, T, is generally *unknown*. To allow for both varying environmental parameters and sample impurity, the sinusoidal damping constants and the echo damping constants, $\beta_k^{(p)}$ and $\eta_k^{(p)}$, are commonly modelled as unknown. For many compounds,

[1] Quadrupolar nuclei are found in around half of all known elements.

[2] The term refocusing pulse refers to the pulse, for example in a pulsed-spin locking (PSL) sequence, which refocuses the transverse magnetisation to produce an echo.

such as for trinitrotoluene (TNT), the frequency shifting functions, at likely operating temperatures, can be well modelled as [12, 13]

$$\omega_k^{(p)}(T) = a_k^{(p)} - b_k^{(p)} T, \tag{3}$$

where $a_k^{(p)}$ and $b_k^{(p)}$ are given constants (It is noted that the frequency shifting functions for different crystalline structures are, in general, different [4, 10, 11]). Furthermore, information about the relative amplitudes is often available for a given examined sample and experimental setup [4, 8, 9, 10, 11]. To exploit this knowledge, we will let

$$\alpha_k^{(p)} = \rho \kappa_k^{(p)}, \tag{4}$$

where ρ and $\kappa_k^{(p)}$ denote the common scaling constant due to the signal power and the kth a priori known relative amplitude associated with the pth polymorph, respectively. We may concatenate the P relative complex amplitude vectors to form

$$\boldsymbol{\kappa} = \left[\begin{array}{ccc} (\boldsymbol{\kappa}^{(1)})^T & \dots & (\boldsymbol{\kappa}^{(P)})^T \end{array} \right]^T, \tag{5}$$

where $\boldsymbol{\kappa}^{(p)}$ is formed from the $d^{(p)}$ relative amplitudes associated with the pth polymorph. As already noted, the assumed relative amplitudes may differ from the actual (observed) ones. To allow for such uncertainties, we follow the approach outlined in [8, 9], which considers the case when the *assumed* amplitude vector, here denoted $\boldsymbol{\kappa}_a$, and the *actual* amplitude vector, $\boldsymbol{\kappa}$, belong to an uncertainty hypersphere with radius $\sqrt{\varepsilon}$, i.e.,

$$\left\| \boldsymbol{\kappa} - \boldsymbol{\kappa}_a \right\|_2^2 \leq \varepsilon, \tag{6}$$

where the kth component of $\boldsymbol{\kappa}$ may be written as [8, 9]

$$\kappa_k = (|\kappa_{a,k}| + \Delta_k^m) e^{i(\angle \kappa_{a,k} + \Delta_k^p)}, \tag{7}$$

with $|\kappa_{a,k}|$ and $\angle \kappa_{a,k}$ denoting the assumed magnitude and phase components of the kth complex amplitude, respectively, whereas Δ_k^m and Δ_k^p denote the errors in the kth magnitude and phase components, respectively. The magnitude errors, Δ_k^m, are assumed to be independent truncated Gaussian random variables (TGRV) whose distributions are each given by the conditional probability density function (PDF)

$$f\left(\Delta_k^m \middle| \Delta_k^m > -|\kappa_{a,k}| \right) = \frac{f(\Delta_k^m)}{1 - F(-|\kappa_{a,k}|)}, \tag{8}$$

where $f(x)$ is a zero mean Gaussian density, with variance σ_m^2, and $F(x)$ is its corresponding distribution function. Further, the phase errors, Δ_k^p, are assumed to be independent identically distributed (IID) random variables, uniformly distributed over the interval $[-\varphi, \varphi]$, where $0 \leq \varphi \leq \pi$ is selected according to the uncertainty in the phases. The PDF of Δ_k^p is thus given as

$$f(\Delta_k^p) = \left\{ \begin{array}{ll} \frac{1}{2\varphi} & -\varphi < \Delta_k^p \leq \varphi \\ 0 & \text{Otherwise.} \end{array} \right. \tag{9}$$

For simplicity, we define the uncertainty parameter, ν, which couples both the uncertainties in the phases and the magnitudes. For a given value of ν, we set $\varphi = \pi \frac{\nu}{100}$ and $\sigma_m^2 = 0.0001\nu$. To allow the problem to be formulated as a stochastic robust approximation, we also introduce the decomposition of $\boldsymbol{\kappa}$, in (5), as

$$\boldsymbol{\kappa} = \overline{\boldsymbol{\kappa}} + \Delta\boldsymbol{\kappa}, \tag{10}$$

where $\overline{\boldsymbol{\kappa}}$ and $\Delta\boldsymbol{\kappa}$ represent the mean and the (zero mean) random parts of the actual complex scalings (analytical expressions for obtaining $\overline{\boldsymbol{\kappa}}$, $E\{|\Delta\kappa|^2\}$ and ε from assumed complex scalings and uncertainty level are derived in section 3.1). We stress that the assumed complex scalings, $\boldsymbol{\kappa}_a$, may not necessarily coincide with $\overline{\boldsymbol{\kappa}}$.

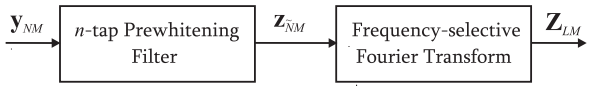

Figure 1: Preprocessing of the measured data.

3. THE REMIQS DETECTOR

We now proceed to develop the proposed REMIQS detector. The measured data vector, formed from M echoes, may be written as

$$\mathbf{y}_{NM} = \left[\begin{array}{ccc} \mathbf{y}_N^T(0) & \dots & \mathbf{y}_N^T(M-1) \end{array} \right]^T, \tag{11}$$

where for the mth echo we have

$$\mathbf{y}_N(m) = \left[\begin{array}{ccc} y_m(t_0) & \dots & y_m(t_{N-1}) \end{array} \right]^T. \tag{12}$$

As depicted in Figure 1, any known noise colouring is removed using an n-tap prewhitening filter, yielding the signal $\mathbf{z}_{\tilde{N}M}$, having $\tilde{N}M$ samples (with $\tilde{N} = N - n$) (see also [5, 10, 11]). Further, as the temperature of the sample can be assumed to lie in a known range, we may, using (3), determine the range of frequencies each of the sinusoidal components may be present in. These frequency regions may be formed as

$$\left\{ \frac{2\pi k_1}{\tilde{N}}, \frac{2\pi k_2}{\tilde{N}}, \dots, \frac{2\pi k_L}{\tilde{N}} \right\}, \tag{13}$$

with $k_1, \dots, k_L$ being L given, not necessarily consecutive, integers selected such that (13) only consists of the possible frequency grid points for each of the $(d^{(1)} + \dots + d^{(P)})$ signal components [5, 10, 11]. Hence, a frequency-selective Fourier transform can be applied to the prewhitened echoes so that the detector considers only these narrow frequency bands. These steps lead to the data model [10, 11]

$$\mathbf{Z}_{LM} = \boldsymbol{\Sigma}\mathbf{g}_\gamma + \mathbf{E}_{LM}, \tag{14}$$

where $\mathbf{E}_{LM}$ represents the noise vector and

$$\mathbf{g}_\gamma = \left[\begin{array}{ccc} \rho\gamma_1 & \dots & \rho\gamma_P \end{array} \right]^T \tag{15}$$

$$\boldsymbol{\Sigma} = \left[\begin{array}{ccc} \tilde{\mathbf{H}}^{(1)}\boldsymbol{\kappa}^{(1)} & \dots & \tilde{\mathbf{H}}^{(P)}\boldsymbol{\kappa}^{(P)} \end{array} \right] \tag{16}$$

$$\tilde{\mathbf{H}}^{(p)} = \left[\begin{array}{c} \mathbf{V}_L^* \mathbf{A}_{\overline{\theta}^{(p)}}^{(p)} \mathbf{B}_0^{(p)} \\ \vdots \\ \mathbf{V}_L^* \mathbf{A}_{\overline{\theta}^{(p)}}^{(p)} \mathbf{B}_{M-1}^{(p)} \end{array} \right] \tag{17}$$

$$\mathbf{B}_m^{(p)} = \operatorname{diag}\left\{ \begin{array}{ccc} e^{-\eta_1^{(p)} m\mu} & \dots & e^{-\eta_d^{(p)} m\mu} \end{array} \right\}, \tag{18}$$

with $\overline{\theta}^{(p)} = \left[\begin{array}{ccc} \tau & \beta^{(p)} & \eta^{(p)} \end{array} \right]$ being the vector containing the nonlinear parameters and

$$\mathbf{A}_{\overline{\theta}^{(p)}}^{(p)} = \left[\begin{array}{ccc} C(\lambda_1^{(p)}) S_{1,t_n}^{(p)} & \cdots & C(\lambda_{d^{(p)}}^{(p)}) S_{d^{(p)},t_n}^{(p)} \\ \vdots & \ddots & \vdots \\ C(\lambda_1^{(p)}) S_{1,\tilde{t}_{sp}}^{(p)} & \cdots & C(\lambda_{d^{(p)}}^{(p)}) S_{d^{(p)},\tilde{t}_{sp}}^{(p)} \\ C(\tilde{\lambda}_1^{(p)}) S_{1,\tilde{t}_{sp}+1}^{(p)} & \cdots & C(\tilde{\lambda}_{d^{(p)}}^{(p)}) S_{d^{(p)},\tilde{t}_{sp}+1}^{(p)} \\ \vdots & \ddots & \vdots \\ C(\tilde{\lambda}_1^{(p)}) S_{1,t_{N-1}}^{(p)} & \cdots & C(\tilde{\lambda}_{d^{(p)}}^{(p)}) S_{d^{(p)},t_{N-1}}^{(p)} \end{array} \right] \tag{19}$$

$$S_{k,t}^{(p)} = e^{-\beta_k^{(p)}|t - t_{sp}|} e^{[i\omega_k^{(p)}(T) - \eta_k^{(p)}]t} \tag{20}$$

where $\tilde{t}_{sp}$ is the closest data point such that $\tilde{t}_{sp} \leq t_{sp}$. Furthermore, $C(\lambda_k^{(p)})$ and $C(\tilde{\lambda}_k^{(p)})$ represent the complex scalings due to the prewhitening operation with $C(\lambda)$ denoting the AR prewhitening filter and $\lambda_k^{(p)} = e^{i\omega_k^{(p)}(T)+\beta_k^{(p)}-\eta_k^{(p)}}$, $\tilde{\lambda}_k^{(p)} = e^{i\omega_k^{(p)}(T)-\beta_k^{(p)}-\eta_k^{(p)}}$ (see [6, 10, 11] for further details). Finally, the frequency-selective Fourier transform matrix, $\mathbf{V}_L^*$, is formed using (13) as

$$\mathbf{V}_L = \left[\mathbf{v}_{k_1} \dots \mathbf{v}_{k_L}\right] \quad (21)$$

$$\mathbf{v}_{k_j} = \left[\begin{array}{cccc} 1 & e^{\frac{i2\pi k_j}{N}} & \dots & e^{\frac{i2\pi k_j(N-1)}{N}} \end{array}\right]^T. \quad (22)$$

Using (10) in (16), we may decompose Σ into its mean and uncertainty matrices, i.e.,

$$\Sigma = \bar{\Sigma} + \mathbf{U}, \quad (23)$$

where

$$\bar{\Sigma} = \left[\begin{array}{cccc} \tilde{\mathbf{H}}^{(1)}\bar{\kappa}^{(1)} & \dots & \tilde{\mathbf{H}}^{(P)}\bar{\kappa}^{(P)} \end{array}\right] \quad (24)$$

$$\mathbf{U} = \left[\begin{array}{cccc} \tilde{\mathbf{H}}^{(1)}\Delta\kappa^{(1)} & \dots & \tilde{\mathbf{H}}^{(P)}\Delta\kappa^{(P)} \end{array}\right]. \quad (25)$$

To determine the unknown parameter vector $\mathbf{g}_\gamma$, we form the stochastic robust least squares (SRLS) problem, (26), given at the top of next page, where

$$\mathbf{P} = E\{\mathbf{U}^*\mathbf{U}\}, \quad (27)$$

and $\mathbf{P}^{\frac{1}{2}}$ denotes the Hermitian square root of $\mathbf{P}$. Below, in section 3.1, we discuss how to form $\mathbf{P}$ using the assumed level of uncertainty. The SRLS estimate of $\mathbf{g}_\gamma$ minimizing (26) is given by [14]

$$\hat{\mathbf{g}}_\gamma = \left(\bar{\Sigma}^*\bar{\Sigma} + \mathbf{P}\right)^{-1}\bar{\Sigma}^*\mathbf{Z}_{LM}. \quad (28)$$

It should be stressed that as the measured signal is complex, the unstructured estimate $\hat{\mathbf{g}}_\gamma$ is likely complex too, especially in the likely case when there are discrepancies between the model and the measured data. Bearing this in mind, we allow for a complex scaling, forming the estimate of γ_k as

$$\hat{\gamma}_k = \frac{\left|[\hat{\mathbf{g}}_\gamma]_k\right|}{\sum_{k=1}^{P}\left|[\hat{\mathbf{g}}_\gamma]_k\right|}. \quad (29)$$

Using $\bar{\mathbf{g}}_\gamma = \left[\begin{array}{cccc} \hat{\gamma}_1 & \dots & \hat{\gamma}_P \end{array}\right]^T$, we can obtain robust estimates of the actual complex scalings κ as a solution to the constrained optimization problem

$$\min_{\kappa}\left\|\rho\mathbf{Q}_{\bar{\mathbf{g}}_\gamma}\kappa - \mathbf{Z}_{LM}\right\|_2^2 \text{ subject to } \left\|\kappa - \kappa_a\right\|_2^2 \leq \varepsilon, \quad (30)$$

where the data matrix $\mathbf{Q}_{\bar{\mathbf{g}}_\gamma}$ is formed from the nonlinear parameters

$$\bar{\theta} = \left[\begin{array}{cccccccc} T & \beta^{(1)} & \dots & \beta^{(P)} & \eta^{(1)} & \dots & \eta^{(P)} \end{array}\right]^T, \quad (31)$$

and the estimate $\bar{\mathbf{g}}_\gamma$ as

$$\mathbf{Q}_{\bar{\mathbf{g}}_\gamma} = \left[\begin{array}{cccc} \hat{\gamma}_1\tilde{\mathbf{H}}^{(1)} & \dots & \hat{\gamma}_P\tilde{\mathbf{H}}^{(P)} \end{array}\right]. \quad (32)$$

As shown in [8,9], the minimization in (30) can be solved using the singular value decomposition of $\mathbf{Q}_{\bar{\mathbf{g}}_\gamma}$, providing the robust estimate $\hat{\kappa}$. Given these estimates, the nonlinear parameters, $\bar{\theta}$, can be found by the maximization

$$\max_{\theta} \ \mathbf{Z}_{LM}^*\hat{\mathbf{Z}}_{LM} \ , \quad (33)$$

where $\hat{\mathbf{Z}}_{LM} = \hat{\rho}\mathbf{Q}_{\bar{\mathbf{g}}_\gamma}\hat{\kappa}$ and $\hat{\rho} = (\mathbf{Q}_{\bar{\mathbf{g}}_\gamma}\hat{\kappa})^\dagger\mathbf{Z}_{LM}$. Finally, using the $\bar{\theta}$ maximizing (33), the test statistic is formed as [15]

$$T(\mathbf{Z}_{LM}) = (LM-1)\frac{\mathbf{Z}_{LM}^*\hat{\mathbf{Z}}_{LM}}{\mathbf{Z}_{LM}^*\mathbf{Z}_{LM} - \mathbf{Z}_{LM}^*\hat{\mathbf{Z}}_{LM}}. \quad (34)$$

The signal component is deemed present if and only if

$$T(\mathbf{Z}_{LM}) > \vartheta, \quad (35)$$

and otherwise not, where ϑ is a predetermined threshold value reflecting the acceptable probability of false alarm.

3.1 Derivation of the Matrix P

To form the SRLS estimate of $\hat{\mathbf{g}}_\gamma$ in (28), one needs an expression for the covariance matrix of the uncertainty, $\mathbf{P}$, defined in (27). To form this we note that the *mp:th* block vector of the uncertainty matrix $\mathbf{U}$ can be expressed as

$$[\mathbf{U}]_{mp} = \mathbf{V}_L^*\mathbf{A}_{\bar{\theta}^{(p)}}^{(p)}\mathbf{B}_m^{(p)}\Delta\kappa^{(p)}, \quad (36)$$

with $m = 0, \dots, M-1$ and $p = 1, \dots, P$. The *js:th* element of the matrix $\mathbf{P}$ can thus be written as

$$\mathbf{P}_{js} = E\left\{\sum_{m=0}^{M-1}[\mathbf{U}]_{mj}^*[\mathbf{U}]_{ms}\right\}. \quad (37)$$

Using the assumption that all the uncertainties are uncorrelated and zero mean, it is easy to show that we get $\mathbf{P}_{js} = 0$ for $j \neq s$, while the diagonal elements can be expressed as

$$\mathbf{P}_{jj} = \sum_m\sum_q\sum_r\left|\phi_{qr}^{(m)}\right|^2 E\left\{\left|\Delta\kappa_r^{(j)}\right|^2\right\}, \quad (38)$$

where $q = 1, \dots, P$, $r = 1, \dots, P$ and

$$\phi_{qr}^{(m)} = \left[\mathbf{V}_L^*\mathbf{A}_{\bar{\theta}^{(j)}}^{(j)}\mathbf{B}_m^{(j)}\right]_{qr}. \quad (39)$$

This indicates that one only requires the mean and variance of the uncertainties in order to evaluate (28). Using (6)-(10), these may be determined as [16]

$$E\{\Delta_k^m\} = \frac{\sigma_m}{\sqrt{2\pi}}e^{-(\Gamma_l)^2} \quad (40)$$

$$E\left\{(\Delta_k^m)^2\right\} = \sigma_m\frac{le^{-(\Gamma_l)^2}}{\sqrt{2\pi}} + \sigma_m^2\frac{erf(\Gamma_l)-1}{2}, \quad (41)$$

where $l = -|\kappa_{a,k}|$ is the lower limit of the truncated distribution in (8), $\Gamma_l = \left[\frac{l}{\sigma_m\sqrt{2}}\right]$ and $erf(x) = \frac{2}{\sqrt{(\pi)}}\int_0^x e^{-t^2}dt$. Furthermore, the mean of the uncertain phase part can be expressed as

$$E\{e^{i\Delta_k^p}\} = \int_{-\varphi}^{\varphi}e^{i\Delta_k^p}f(\Delta_k^p)d\Delta_k^p = \frac{sin(\varphi)}{\varphi}. \quad (42)$$

$$\hat{\mathbf{g}}_\gamma = \arg\min_{\mathbf{g}_\gamma} E\left\{ \left\| \mathbf{Z}_{LM} - \Sigma \mathbf{g}_\gamma \right\|_2^2 \right\} = \arg\min_{\mathbf{g}_\gamma} \left\{ \mathbf{g}_\gamma^* \left(\bar{\Sigma}^* \bar{\Sigma} + (\mathbf{P}^{\frac{1}{2}})^* (\mathbf{P}^{\frac{1}{2}}) \right) \mathbf{g}_\gamma - \mathbf{Z}_{LM}^* \bar{\Sigma} \mathbf{g}_\gamma - \mathbf{g}_\gamma^* \bar{\Sigma}^* \mathbf{Z}_{LM} + \mathbf{Z}_{LM}^* \mathbf{Z}_{LM} \right\} \quad (26)$$

Using (40)-(42), the mean $\bar{\kappa}_k = E\{\kappa_k\}$, and the variance of the uncertain part $\Delta\kappa_k$, can be conveniently derived as

$$\bar{\kappa}_k = \left(|\kappa_{a,k}| + E\{\Delta_k^m\} \right) \frac{sin(\varphi)}{\varphi} e^{i\angle\kappa_{a,k}} \quad (43)$$

$$E\left\{ |\Delta\kappa_k|^2 \right\} = E\left\{ |\kappa_k - \bar{\kappa}_k|^2 \right\} \quad (44)$$

$$= |\kappa_{a,k}|^2 + E\left\{ (\Delta_k^m)^2 \right\} + 2|\kappa_{a,k}| E\{\Delta_k^m\} - |\bar{\kappa}_k|^2. \quad (45)$$

Finally, based on the constraint (6), a reasonable way to form ε could be

$$\varepsilon = \left\| \kappa - \kappa_a \right\|_2^2 = \sum_{k=1}^{\ell} \left| \kappa_k - \kappa_{a,k} \right|^2, \quad (46)$$

with κ defined as in (7) and $\ell = \sum_{p=1}^{P} d^{(p)}$. The mean value of ε for a given uncertainty level can then be evaluated as

$$E\{\varepsilon\} = \sum_{k=1}^{\ell} E\left\{ \left| \kappa_k - \kappa_{a,k} \right|^2 \right\}, \quad (47)$$

with each term given by

$$E\left\{ |\kappa_k - \kappa_{a,k}|^2 \right\} = 2|\kappa_{a,k}|^2 + E\left\{ (\Delta_k^m)^2 \right\} + 2|\kappa_{a,k}| E\{\Delta_k^m\} - 2|\kappa_{a,k}||\bar{\kappa}_k|. \quad (48)$$

These relations together ensure that using the assumed complex scalings and uncertainty level, we can obtain all the parameters needed for the implementation of the REMIQS detector.

4. LS-FHETAML

As a reference method, we will here briefly formulate the Least Squares FHETAML (LS-FHETAML) detector, formed from the detector in [10,11], that does not use the a priori available information about the complex amplitudes and considers them fully unknown. Using

$$\mathbf{R}_{\bar{\theta}} = \left[\tilde{\mathbf{H}}^{(1)} \quad \dots \quad \tilde{\mathbf{H}}^{(P)} \right], \quad (49)$$

and defining ϕ as the vector containing the unknown linear parameters κ and $\mathbf{g}_\gamma$, the least square estimate of ϕ can be formed as

$$\hat{\phi} = \arg\min_{\phi} \left\| \mathbf{R}_{\bar{\theta}} \phi - \mathbf{Z}_{LM} \right\|_2^2 = \left(\mathbf{R}_{\bar{\theta}}^* \mathbf{R}_{\bar{\theta}} \right)^{-1} \mathbf{R}_{\bar{\theta}}^* \mathbf{Z}_{LM}. \quad (50)$$

The detector is then formed using $\hat{\mathbf{Z}}_{LM} = \mathbf{R}_{\bar{\theta}} \hat{\phi}$ in (33)-(35).

5. NUMERICAL EXAMPLES

In this section, we examine the performance of the proposed detector using simulated NQR data. TNT is a common explosive in landmines and currently poses a great challenge for the detection of landmines using NQR. Detection of TNT is complicated by the existence of at least two polymorphic forms, monoclinic and orthorhombic, with different NQR properties, e.g., different temperature shifting functions. Landmines often contain a mixture of these two forms, the proportions of which can vary between landmines (and over time in a given landmine) as the metastable

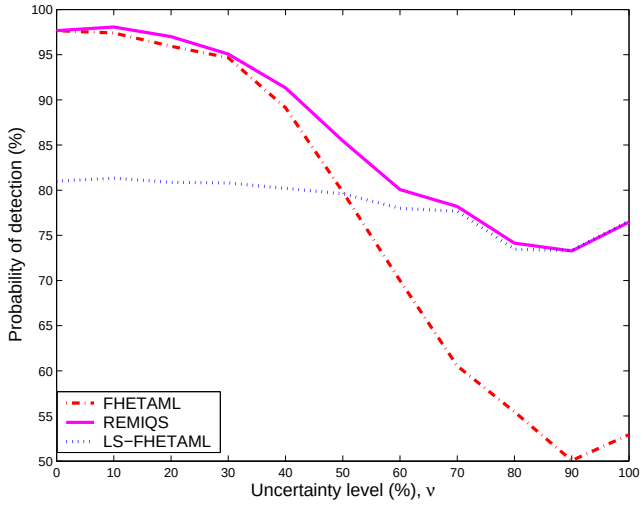

Figure 2: Plots illustrating p_d as a function of the uncertainty level, ν, for $p_f = 1\%$.

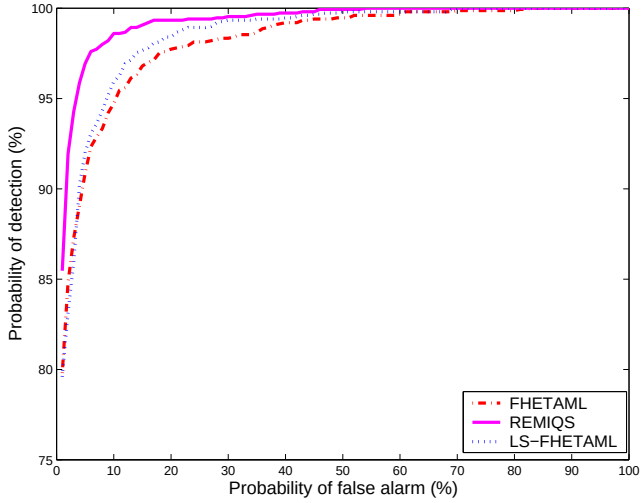

Figure 3: ROC curves comparing the detectors for $\nu = 50\%$.

orthorhombic form may change slowly to the more stable (at room temperature) monoclinic phase. Herein, we will limit our attention to examine two of the polymorphic forms of TNT, i.e., $P = 2$, namely the monoclinic ($p = 1$) and the orthorhombic ($p = 2$) polymorphs. The data was generated using (1)-(3) together with the temperature shifting functions and parameter values as recorded in [11]. The number of Monte-Carlo simulations was 1500 and the SNR was -26 dB, where SNR is defined as SNR $= \sigma_e^{-2}\sigma_s^2$, with σ_e^2 and σ_s^2 denoting the power of the noise and the noise-free signal, respectively. In the following analysis, we compare the proposed REMIQS algorithm to the non-robust hybrid FHETAML algorithm, presented in [10, 11], together with the LS-FHETAML detector derived in section 4. The detectors used the following search regions (see, e.g., [6] for further explanations on how to choose the search regions); the search region over temperature was selected as $T = [290, 310]$ K (in 100 steps), the common echo

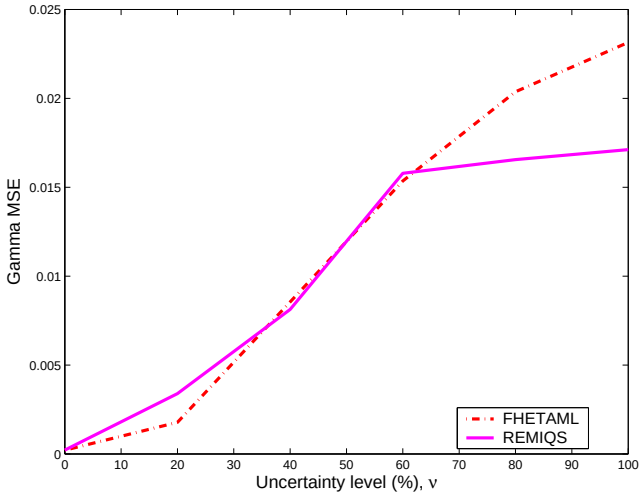

Figure 4: Mean square error in $\hat{\gamma}_1$ as a function of uncertainty level ν.

damping parameters ${\eta_0}^{(1)}$ and ${\eta_0}^{(2)}$ both used the search region $[0.0001, 0.0004]$ (in 100 steps). Finally, the search regions used for the common sinusoidal damping parameters ${\beta_0}^{(1)}$ and ${\beta_0}^{(2)}$ were $[0.001, 0.01]$ and $[0.02, 0.03]$ (both in 100 steps), repectively. Figure 2 illustrates the probability of detection (p_d) as a function of the uncertainty level, ν, for a probability of false alarm (p_f) of 1%. For each uncertainty level, the mean ε was evaluated using (47) and (48). The figure shows that the proposed robust detector outperforms the other detectors for all uncertainty levels; this as the REMIQS detector is able to incorporate prior knowledge, whilst also allowing for uncertainties in it. The figure also shows that at low uncertainty levels the LS-FHETAML gives the worst performance, since it fails to utilize the available information. On the other hand, the performance of FHETAML detector deteriorates rapidly with increasing levels of uncertainty in the assumed kappas. Figure 3 illustrates the ROC curves for the different detectors at an uncertainty level of 50%. The figure clearly shows the beneficial performance of REMIQS over the other detectors. The ability of the proposed detector to estimate the proportions of the polymorphs at various uncertainty levels was also analyzed. As quantification of polymorphs in pharmaceutical application allows for higher SNR than typically can be expected in demining scenarios, we choose to increase the used SNR to 0 dB when examining the quality of the quantification (similar results hold also for lower SNRs). Figure 4 shows the MSE plots for the $\hat{\gamma}_1$ estimates at different levels of uncertainty. As is clear from the plot, REMIQS provides better estimates at medium to high levels of uncertainties.

6. ACKNOWLEDGEMENT

The authors are grateful to Professor John A. S. Smith at King's College London for his invaluable help on NQR, and Erik Gudmundson at Uppsala University for useful discussions. Part of the computations was performed on UPPMAX resources under Project p2005010.

REFERENCES

[1] A. N. Garroway, M. L. Buess, J. B. Miller, B. H. Suits, A. D. Hibbs, A. G. Barrall, R. Matthews, and L. J. Burnett, "Remote sensing by nuclear quadrupole resonance," *IEEE Trans. Geosciences and Remote Sensing*, vol. 39, no. 6, pp. 1108–1118, june 2001.

[2] R. M. Deas, I. A. Burch, and D. M. Port, "The Detection of RDX and TNT Mine like Targets by Nuclear Quadruple Resonance," in *Detection and Remediation Technologies for Mines and Minelike Targets, Proc. of SPIE*, vol. 4742, 2002, pp. 482–489.

[3] E. Balchin, D. J. Malcolme-Lawes, I. J. F. Poplett, M. D. Rowe, J. A. S. Smith, G. E. S. Pearce, and S. A. C. Wren, "Potential of Nuclear Quadrupole Resonance in Pharmaceutical Analysis," *Analytical Chemistry*, vol. 77, pp. 3925–3930, 2005.

[4] A. Jakobsson, M. Mossberg, M. Rowe, and J. A. S. Smith, "Exploiting Temperature Dependency in the Detection of NQR Signals," *IEEE Transactions on Signal Processing*, vol. 54, no. 5, pp. 1610–1616, May 2006.

[5] ——, "Frequency Selective Detection of Nuclear Quadrupole Resonance Signals," *IEEE Trans. Geoscience and Remote Sensing*, vol. 43, no. 11, pp. 2659–2665, November 2005.

[6] S. D. Somasundaram, A. Jakobsson, J. A. S. Smith, and K. Althoefer, "Exploiting spin echo decay in the detection of nuclear quadrupole resonance signals," *IEEE Trans. Geoscience and Remote Sensing*, to appear.

[7] L. V. Anferova and V. S. Grechiishkin, "Physics of magnetic phenomena - use of the bohr principle for detecting nqr signals from mines," *Russian Physics Journal*, vol. 48, pp. 148–155, 2005.

[8] S. D. Somasundaram, A. Jakobsson, and E. Gudmundson, "Robust NQR Signal Detection," in *32nd IEEE International Conference on Acoustics, Speech and Signal Processing*, Honolulu, April 15-20 2007.

[9] ——, "Robust NQR Signal Detection Allowing for Amplitude Uncertainties," submitted to IEEE Trans. Signal Processing.

[10] S. D. Somasundaram, A. Jakobsson, and J. A. S. Smith, "Frequency Selective Detection of NQR Signals in the Presence of Multiple Polymorphic Forms," in *14th European Signal Processing Conference*, Florence, September 4-8, 2006.

[11] ——, "Analysis of Nuclear Quadrupole Resonance Signals from Mixtures," submitted to *Elsevier, Signal Processing*.

[12] J. A. S. Smith, M. D. Rowe, R. M. Deas, and M. J. Gaskell, "Nuclear Quadrupole Resonance Detection of Landmines," in *Conference Requirements and Technologies for the Detection, Removal and Neutralization of Landmines and UXO*, vol. 2, September 2003, pp. 715–721.

[13] J. A. S. Smith and M. D. Rowe, "NQR testing method and apparatus," *Patent WO9945409*, 1999.

[14] S. Boyd and L. Vandenbeghe, *Convex Optimization*. Cambridge University Press, 2004.

[15] S. M. Kay, *Fundamentals of Statistical Signal Processing, Volume II: Detection Theory*. Englewood Cliffs, N.J.: Prentice-Hall, 1998.

[16] J. W. Jawitz, "Moments of truncated continuous univariate distributions," *Advances in Water Resources*, vol. 27, pp. 269–281, 2004.